Appendix A: Ctene kinematics and swimming efficiency

Kinematics

We model each ctene as a flat plate which oscillates unidirectionally with a time-varying height, such that the tip of the plate traces out an elliptical trajectory (see Figure 7 in the manuscript). To define the beating kinematics, we first derive expressions to construct the elliptical trajectory for the plate tip—namely, finding the semimajor and semiminor axes (a and b) as function of the spatial asymmetry (*Sa*) and the ctene length (l). In equation (2), A_o is defined as the largest possible area of an ellipse contained within the reachable area of the ctene, which is 0.77 times the reachable area of a rigid, nonbending ctene (the half circle with area $\pi l^2/2$). Substituting into equation (2) we get $Sa = A_e/0.385\pi l^2$, where A_e is the area of the elliptical tip trajectory ($A_e = \pi ab$). From this we can calculate the semiminor axis b as

$$b = 0.385\frac{l^2}{a}Sa \qquad (A.1)$$

To calculate the semimajor axis a, we must include the stroke amplitude (Φ). Figure 7B shows that the starting and ending points of the power stroke are defined by Φ and the perimeter of the half circle with radius l. Focusing on a triangle formed by the origin, the center of the ellipse, and a major axis vertex we can calculate the semimajor axis length and the y-coordinate of the center of the ellipse as:

$$a = l\sin(\Phi/2) \qquad (A.2)$$

$$y_c = l\cos(\Phi/2) \qquad (A.3)$$

The position of the plate tip is given by the parametric equations of the ellipse: $x_A = a\cos\theta$ and $y_A = y_c + b\sin\theta$. The tip velocity is given by the corresponding derivatives $\dot{x}_A = -a\dot{\theta}\sin\theta$ and $\dot{y}_A = b\dot{\theta}\cos\theta$. To evaluate the kinematics, we must define expressions for the angular velocity ($\dot{\theta}$) and the angular position (θ) as functions of time. We will assume a constant angular velocity for the power and recovery strokes ($\dot{\theta}_p$ and $\dot{\theta}_r$):

$$\dot{\theta}_p = \frac{\pi}{t_p} \qquad (A.3a)$$

$$\dot{\theta}_r = \frac{\pi}{t_r} \qquad (A.3b)$$

The power and recovery stroke time are easily calculated from the temporal asymmetry and cycle period: $t_r = T(Ta + 1)/2$ and $t_p = T - t_r$. Lastly, $\theta(t)$ can be continuously evaluated for as many cycles as needed following this piecewise-defined function:

$$\theta(t) = \begin{cases} \dot{\theta}_p[t - (mt_r)] + m\pi & for \quad mT \le t \le mT + t_p \\ (m+1)\pi + \dot{\theta}_r[t - (m+1)t_p] & for \quad mT + t_p < t \le (m+1)T \end{cases} \qquad (A.4)$$

where m is the cycle number ($m = 0,1,2,3,\ldots$). Equations A.1 to A.4, define the kinematics of the model.

Swimming efficiency

The swimming efficiency ($\eta = P_o/P_i$) is defined as the ratio between the output power (P_o) to the input power (P_i). These are computed as

$$P_i = \frac{N}{t}\sum_{k=1}^{n}\int_0^t F_p\,[\dot{x}_{\boldsymbol{B}} + \dot{x}_A(t + (k-1)\tau)]dt \qquad (A.5a)$$

$$P_o = \frac{1}{t}\left[\int_0^t F_d\dot{x}_B dt + \int_0^t (m + \alpha\rho V)\ddot{x}_B\dot{x}_B dt\right] \qquad (A.5b)$$

where the summation in A.5a calculates the work done by the *n* ctenes in a row, multiplied by the number of ctene rows ($N = 8$) and divided by the swimming time (t) to obtain power. Equation (A.5b) accounts for the work needed to overcome drag (first integral) and the work expended to overcome the acceleration reaction force and produce the body's own acceleration (second integral) (Daniel, 1983).

Appendix B: Drag coefficients

Drag coefficient for an oscillating plate at intermediate Re

From (Shih and Buchanan, 1971) we obtain an empirical expression for the drag coefficient of an oscillating plate, appropriate for Reynolds numbers between 1.01 and 1057.

$$C_A = 15Pe^{-0.5}\exp\left(\frac{1.88}{{R_e}^{0.547}}\right) \qquad (B.1)$$

where Pe is the period parameter and is defined as $Pe = (\dot{x}_{A,max} - \dot{x}_{\boldsymbol{B}})(T)/w$, and the Reynolds number for this equation is defined as $Re = (\dot{x}_{A,max} - \dot{x}_{\boldsymbol{B}})w/\nu$.

Drag coefficient for a prolate spheroid at intermediate Re

From (Loth, 2008) we obtain an expression for the drag coefficient of a prolate spheroid whose major axis is aligned with the flow:

$$C_B = C_{shape}\left[\frac{24}{{Re_B}^*}\left(1 + 0.15{Re_B}^{*0.687}\right) + \frac{0.42}{1 + \frac{42{,}500}{{Re_B}^{*1.16}}}\right] \qquad (B.2)$$

$${Re_B}^* = \frac{C_{shape}}{f_{shape}}\left(\frac{\dot{x}_B d}{\nu}\right)$$

$$f_{shape} = \frac{(4/3){\alpha_s}^{-\frac{1}{3}}(1 - {\alpha_s}^2)}{\alpha_s - \frac{(2{\alpha_s}^2 - 1)\ln(\alpha_s + \sqrt{{\alpha_s}^2 - 1})}{\sqrt{{\alpha_s}^2 - 1}}}$$

$$C_{shape} = 1 + 0.7\sqrt{\left({A_{surf}}^{*} - 1\right)} + 2.4\left({A_{surf}}^{*} - 1\right)$$

$${A_{surf}}^{*} = \frac{1}{2{\alpha_s}^{\frac{2}{3}}}\left[1 + \frac{\alpha_s}{\sqrt{1 - {\alpha_s}^{-2}}} sin^{-1}\left(\sqrt{1 - {\alpha_s}^{-2}}\right)\right]$$

where α_s is the aspect ratio of the body $\alpha_s \equiv L_b/d$.

Appendix C: Swimming model verification

To verify that our analytical model predicts forces that are comparable to those generated by the real animal it is meant to represent, we will compare the model to actual freely swimming ctenophores. Our model considers a ctenophore swimming in a straight line, with a constant beat frequency, whose body orientation is aligned with the swimming trajectory (heading angle of zero degrees). We consider two swimming trajectories that resemble the modeled situation—one steady swimming animal, and one animal which accelerates from near rest.

Swimming tracking of Bolinopsis vitrea

We performed 3D kinematic tracking of freely swimming ctenophores at BIOS. The experimental setup is described in two existing studies (Karakas *et al.*, 2018; Karakas, Maas and Murphy, 2020);these data are contemporary with the latter study. In three simultaneous orthogonal views of a freely swimming animal, we tracked the apical organ and the tentacular bulbs (Figure 1) using DLTdv8 (Hedrick, 2008). The beat frequency and phase lag were measured manually, counting the beat period of two neighboring ctenes from each visible ctene row on the three videos. An example of a fully tracked unidirectional trajectory is shown in Figure 1. From the measured trajectory, we calculate the swimming speed. Figure 2 shows examples of two possible straight swimming scenarios: steady and unsteady (acceleration from near rest) body speed. Relevant morphometric and kinematic parameters can be found in Table I.

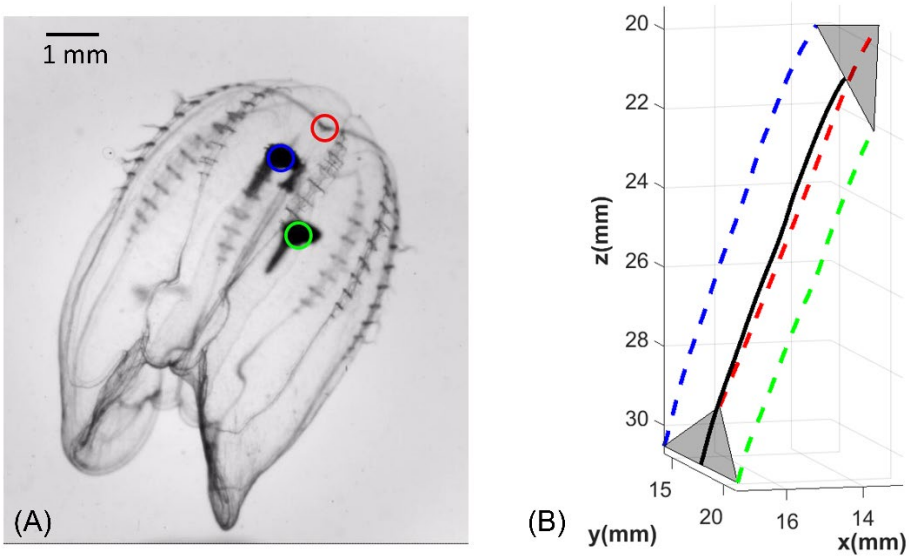

Figure 1. Three-dimensional tracking of freely swimming ctenophores. (A) Tracked points: apical organ (red) and tentacular bulbs (blue and green). (B) An example of a reconstructed trajectory; the black line is the swimming trajectory.

Table I. Morphometric and kinematic measurements of observed animals (mean ± one standard deviation)

Body length (mm)	Body width (mm)	No. Ctenes	Ctene length (mm)	Phase Lag (%)	Beat frequency (Hz)
6.24	5.36	9	0.38	13.5±4.82	28.97±1.74
8.18	6.25	9	0.41	17.1±3.52	27.89±0.98

Swimming speed experimental vs. mathematical model

Based on these experimental observations, we run the swimming model (equation 6 in the manuscript) with the values listed in Table I, using the mean value for P_L and f. We also need to set values for Φ, Sa, and Ta; however, these are impossible to measure in our recordings. To measure Φ and Sa together with whole-body trajectories, we need a perfectly aligned view and an extremely high-resolution sensor given the range of sizes that must be resolved. For Ta, our 600 fps recordings are not resolved enough in time. We therefore estimate Φ, Sa, and Ta from our experimental observations (see Figure 6 and Table IV in the manuscript). The stroke amplitude shows almost no variation in our measurements; thus, we set it to the mean observed value 112°. Shaded areas in Figure 2 represent solutions for the entire Sa-Ta space considered in the manuscript ($0.1 < Sa < 0.6$ and $0.1 < Ta < 0.6$). Blue lines in Figure 2 are the combinations of Sa and Ta that best predict the observed animal speed (red line), yielding $Sa = 0.55$ and $Ta = 0.35$ for the unsteady case and $Sa = 0.3$ and $Ta = 0.2$ for the steady case. These values of Sa and Ta are within the experimental range observed in Figure 6.

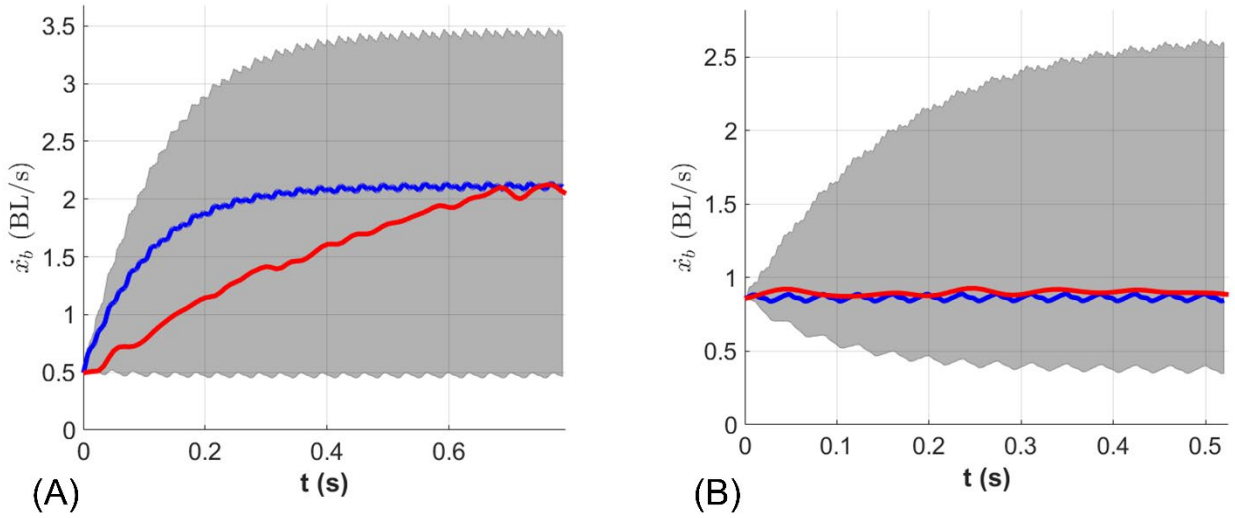

Figure 2. Comparison between experimental (red line) and modeled (blue line) swimming speed. The shaded area represents all Sa-Ta combinations considered in Figures 8-10 in the manuscript. (A) shows an animal accelerating from near rest. The modeled speed (blue line) has $Sa = 0.55$ and $Ta = 0.35$. (B) shows an animal swimming at a steady speed. The modeled speed (blue line) has $Sa = 0.3$ and $Ta = 0.2$.

This highly simplified swimming model permits a high-resolution parametric study of the first-order effects of varying spatiotemporal asymmetry in metachronal swimming. The agreement between observed and predicted swimming speeds shown in Figure 2 verifies that the model can produce similar propulsive forces as those generated by the animals.

References

Daniel, T. L. (1983) 'Mechanics and energetics of medusan jet propulsion', *Canadian Journal of Zoology*, 61(6), pp. 1406–1420. doi: 10.1139/z83-190.

Hedrick, T. L. (2008) 'Software techniques for two- and three-dimensional kinematic measurements of biological and biomimetic systems', *Bioinspiration and Biomimetics*. IOP Publishing, 3(3), p. 034001. doi: 10.1088/1748-3182/3/3/034001.

Karakas, F. *et al.* (2018) 'Using a shell as a wing: Pairing of dissimilar appendages in atlantiid heteropod swimming', *Journal of Experimental Biology*. Company of Biologists Ltd, 221(23). doi: 10.1242/jeb.192062.

Karakas, F., Maas, A. E. and Murphy, D. W. (2020) 'A novel cylindrical overlap-and-fling mechanism used by sea butterflies', *The Journal of experimental biology*. NLM (Medline), 223(15). doi: 10.1242/jeb.221499.

Loth, E. (2008) 'Drag of non-spherical solid particles of regular and irregular shape', *Powder Technology*. Elsevier, 182(3), pp. 342–353. doi: 10.1016/j.powtec.2007.06.001.

Shih, C. C. and Buchanan, H. J. (1971) 'The drag on oscillating flat plates in liquids at low Reynolds numbers', *Journal of Fluid Mechanics*. Cambridge University Press, 48(2), pp. 229–239. doi: 10.1017/S0022112071001563.